Downscaling ESA CCI Soil Moisture Based on Soil and Vegetation Component Temperatures Derived From MODIS Data

Chengyun Song, Guangcheng Hu, Yanli Wang, and Xueshan Qu

***Abstract*—The European Space Agency's Climate Change Initiative (ESA CCI) soil moisture could provide long-time microwave-retrieved soil moisture data but is limited to regional applications due to the low resolution (25 km). A new method of downscaling ESA CCI soil moisture to 1 km is presented in this study. First, the soil and vegetation component temperatures (SVCT) were estimated using MODIS land surface temperature and normalized difference vegetation index (NDVI) data. Following this, the relationship between ESA CCI soil moisture and 1-km SVCT was constructed based on the negative linear relationship between the temperature vegetation dryness index (TVDI) and soil moisture. The dry and wet lines used to estimate TVDI need not to be obtained in the method. The coefficients were obtained directly from 25-km ESA CCI soil moisture and 1-km SVCT by the upscaling algorithm of soil moisture. The method was applied to the Naqu area on the Tibetan Plateau. Downscaled soil moisture was validated with ground measurements collected at five sites within the soil moisture/temperature monitoring network on the central Tibetan Plateau from May to October 2014. The results show that the trend of the time series of the downscaled soil moisture is similar to the ground measurements during this period, and the root-mean-square error is 0.0568 m^3/m^3. The method is suitable for the condition with an NDVI higher than 0.4. The key points of the approach are to obtain SVCT and the relationship between soil moisture and SVCT.**

***Index Terms*—Downscaling, ESA CCI soil moisture, MODIS, soil and vegetation component temperature (SVCT).**

I. Introduction

SOIL moisture is considered an important parameter in the fields of ecology, agriculture, and climate. It also plays an important role in regulating land water, carbon, and the energy cycle [1], [2]. Moreover, soil moisture regulates soil water flux by influencing infiltration and surface runoff [3]. Therefore, it is more useful to monitor soil moisture at regional scales instead of *in situ* measurements. Remote sensing can be used to get continuous data sets on a large scale, and many methods of monitoring soil moisture using remote sensing have been proposed [4]–[6]. Compared with the visible and infrared bands, microwave satellites are sensitive to soil moisture and have a certain penetration to clouds and vegetation. Active and passive microwave satellites are widely used in soil moisture estimation [7], [8].

Today, many active and passive microwave satellite sensors have been used to estimate soil moisture, such as the Advanced Microwave Scanning Radiometer for Earth Observing System (AMSR-E) [9], Advanced Microwave Scanning Radiometer 2 (AMSR2) [10], Soil Moisture and Ocean Salinity (SMOS) [11], Fengyun-3 [12], and Soil Moisture Active Passive (SMAP) [13]. The European Space Agency's Climate Change Initiative (ESA CCI) soil moisture product as one part of CCI is produced by combining the microwave-derived soil moisture to get a longer time and more useful soil moisture product [14], [15]. ESA CCI soil moisture has been applied to many fields, such as agriculture, climatic variables, and precipitation estimations [16], [17].

However, with the low spatial resolution of the microwave radiometer, the resolution of ESA CCI is about 25 km and can be applied at a global scale. Furthermore, fine-scale soil moisture (about 1 km) is needed for applications at a regional scale, such as evapotranspiration modeling, drought monitoring, and farm management. Downscaling low-resolution soil moisture to a finer resolution has become a very meaningful research subject [18].

Research studies on downscaling soil moisture have been done, and the methods can be divided into different strategies according to the auxiliary data used [14]–[17]. First, optical/thermal data are usually used for downscaling soil moisture, such as the empirical statistical analysis based on surface temperature/vegetation index triangular feature space [19]–[21]; disaggregation based on physical, theoretical scale change method [22], [23], the regression-based method [24], or the method based on machine learning [25]. The method based on the vegetation temperature condition index [26] or temperature vegetation dryness index (TVDI) [27] was also proved to be applicable. Meanwhile, many studies applied the normalized difference vegetation index (NDVI) and land surface temperature (LST) gap-filling algorithms to reduce the influence

Manuscript received July 11, 2021; revised October 28, 2021 and December 6, 2021; accepted February 25, 2022. Date of publication March 1, 2022; date of current version March 15, 2022. This work was jointly supported by the Natural Science Foundation of the Anhui Higher Education Institutions of China under Grant KJ2017A072, National Key R&D Program of China under Grant 2017YFD0300402, and the National Natural Science Foundation of China under Grant 41701495. *(Corresponding author: Chengyun Song.)*

Chengyun Song, Yanli Wang, and Xueshan Qu are with the School of Geomatics, Anhui University of Science & Technology, Huainan 232001, China (e-mail: chysong@aust.edu.cn; ylwang@aust.edu.cn; xsqu@aust.edu.cn).

Guangcheng Hu is with the Aerospace Information Research Institute, Chinese Academy of Sciences, Beijing 100101, China (e-mail: hugc@aircas.ac.cn).

Digital Object Identifier 10.1109/JSTARS.2022.3155463

of cloud cover on the soil moisture downscaling methods [28], [29].

Another approach is to use high-resolution active microwave data. The algorithm includes active and passive microwave data fusion method [20]–[32], change detection algorithm [33], [34], and the base-line algorithm, which were provided for SMAP mission [35], [36]. There are also many approaches for downscaling soil moisture using multiple sources of data; Piles *et al.* [37] proposed the method of downscaling SMOS soil moisture using optical/thermal data and L-band brightness temperature. *In situ* soil moisture, topography, soil properties, and other information observed on the ground were also used to disaggregate coarse-resolution soil moisture [38]–[40].

Compared with other methods, the method using optical/thermal data is more feasible for the easy availability of auxiliary data. The downscaling method based on TVDI, which can be estimated with the dry and wet lines of the surface temperature/vegetation index triangular feature space, is proved. However, the surface temperature/vegetation index triangular feature space needs the full range of soil moisture in the study area, and it was not the truth in many cases. The dry and wet lines would not be estimated accurately [41], [42].

The approach in this study is to develop a method to downscale ESA CCI soil moisture based on TVDI using soil and vegetation component temperatures (SVCT) derived from MODIS data. Compared with the method using TVDI, dry and wet lines need not to be estimated in this study. First, SVCT are estimated using MODIS LST and NDVI data based on the hypothesis that the component temperature is close to the neighborhood pixels. Second, the relationship between ESA CCI soil moisture and the 1-km SVCT was constructed based on the negative linear relationship between TVDI and soil moisture. The method is applied to the east area of Naqu and validated with ground measurements from the soil moisture/temperature monitoring network on the central Tibetan Plateau (TP-STMNS).

II. Study Area and Data

A. Study Area

The study area is located in the eastern part of Naqu in the Tibetan Plateau and located between 89°35' –92°45'E and 30°5' –31°45'N [the black rectangle in Fig. 1(a)]. The topography of the study area is mainly plateau and hilly terrain; most are round with a gentle slope, with an average altitude of more than 4500 m. The climate is colder and drier with an annual average temperature of −2.9 to 3.4 °C, and the annual sunshine hours are 2400–3200 h. The annual precipitation is more than 400 mm, mainly occurring from June to August. The vegetation is mainly grassland, entering the turning green period from April to June. The vegetation coverage is high and growing well from July to September, and it begins to wither and yellow from late August to mid-October.

B. Data

1) ESA CCI Soil Moisture Data: ESA CCI soil moisture as a part of the climate change initiative can provide a long-time and unified global soil moisture data set. ESA CCI soil moisture has merged passive and active soil moisture products and is divided into passive, active, and combined soil moisture products [14], [15]. The active products include the soil moisture from an active microwave instrument and an advanced scatterometer. The passive products merge the soil moisture from the scanning multichannel microwave radiometer, special sensor microwave imager, tropical rainfall measuring mission microwave imager, AMSR-E, WindSat, and AMSR-2. The combined soil moisture merges the active and passive senor products. The CCI soil moisture is volumetric water content with a 0.25° resolution. There are many versions of soil moisture according to the merge algorithm and data. The combined soil moisture V5.2 is used in this study from May to October 2014 in the study area. ESA CCI soil moisture was downloaded from.[1]

2) MODIS Data: MODIS data are used to estimate SVCT and downscale ESA CCI soil moisture. The MODIS data used included MODIS MYD11A1 daily LST data and MYD13A2 NDVI data. The MYD11A1 product could provide daily LST at 1 km, and the MYD13A2 NDVI product could provide 16-day NDVI at 1 km. The MODIS data were collected from May 1 to October 31 in 2014 from NASA's website.[2]

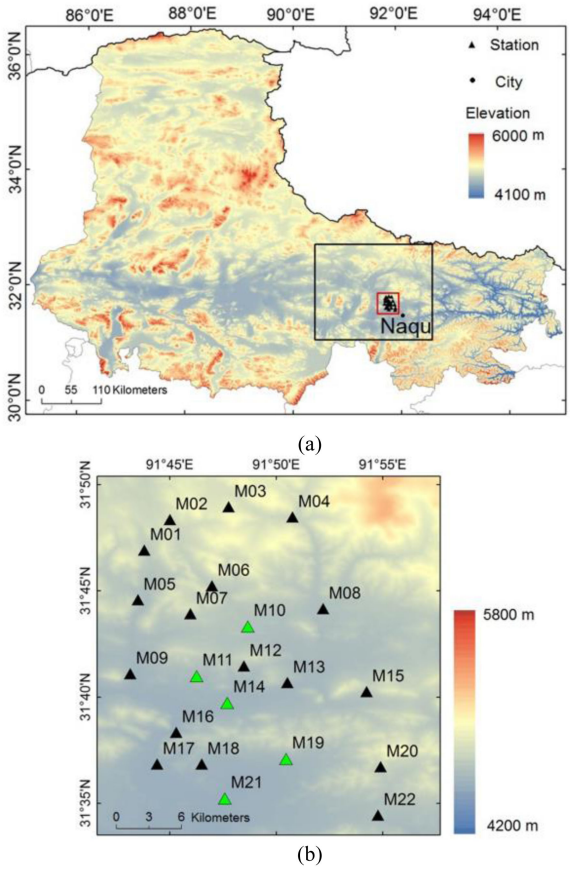

Fig. 1. (a) SRTM DEM of Naqu and the study area (denoted by the black rectangle). (b) Medium-scale network of TP-STMNS (The stations symbolizing green were used to validate the downscaled soil moisture).

[1][Online]. Available: https://www.esa-soilmoisture-cci.org/
[2][Online]. Available: http://ladsweb.nodaps.eosdis.nasa.gov/

3) Ground Observation Data: The ground observation data were collected from TP-SMTMN[3] [43]. The network is located in the northwest of Naqu city. Rolling hills are distributed in the area, and the average elevation is above 4500 m. The surface was frozen from December to February of the following year, and soil moisture partially iced during this period. The network could provide the observation data of the soil temperature and soil moisture at a large scale (1.0°), a medium scale (0.3°), and a small scale (0.1°). The observation depths were 5, 10, 20, and 40 cm, and the observation interval was 30 min. As the resolution of ESA CCI soil moisture is 0.25°, the ground observation data with a depth of 5 cm within the medium scale [see Fig. 1(b)] were selected to compare with the results.

As the distribution of observation stations is scattered, only one observation station is within the coverage range of a 1-km pixel. The five sites (M10, M11, M14, M19, and M21) located in a relatively flat area with a slope of less than 3° were selected [symbolizing the green in Fig. 1(b)] to reduce the difference between ground-measured soil moisture and pixel-derived soil moisture. The *in situ* soil moisture was measured at a depth of 5 cm at the five sites and was compared with the results from May to October 2014.

III. Method

A. Soil and Vegetation Component Temperatures

SVCT play an important role in soil moisture and regional evapotranspiration. According to Stefan–Boltzmann's law and Kirchhoff's law, for vegetation–soil mixed pixel, radiation flux (W) can be expressed as follows:

$$W = \sigma \cdot \varepsilon \cdot T^4 \tag{1}$$

where σ is the Stefan–Boltzmann constant, ε is the emissivity, and T is the surface temperature.

The radiation flux of the pixel can be expressed as a linear combination of vegetation component radiation flux and soil component radiation flux. It can be expressed as follows:

$$\sigma \cdot \varepsilon \cdot T^4 = (1 - f_c) \cdot \sigma \cdot \varepsilon_s \cdot T_s^4 + f_c \cdot \sigma \cdot \varepsilon_v \cdot T_v^4 \tag{2}$$

where f_c is the fractional coverage estimated with the NDVI [37].

For the vegetation–soil mixed pixel, the emissivity of the pixel corresponds to radiation coming from the soil and vegetation. The emissivity of pixel can be express as follows [38]:

$$\varepsilon = (1 - f_c) \cdot \varepsilon_s + f_c \cdot \varepsilon_v. \tag{3}$$

Considering the field measurements by other authors under similar conditions in the 8- to 14-μm spectral region, the values of ε_s and ε_v can be considered as 0.97 and 0.985, respectively, in the study area [38], [39].

When the temperature of the pixel is known and the emissivity of the pixel can be estimated with (3), the following hypotheses were made to obtain the vegetation and soil component temperatures with (2).

1) SVCT of adjacent pixels are close.
2) Vegetation component temperature is lower than soil component temperature in the same pixel.

In the study area, the surface was mainly covered with grassland, and the main soil type was loess. It can be considered that the soil type and vegetation type were consistent within a few kilometers. For the MODIS 1-km LST and NDVI data, it can be considered that hypothesis 1 was true.

According to hypothesis 2, there would be a negative correlation between the surface temperature and vegetation coverage of the pixels, and the temperature value of the pixel should have been reduced with the increase in the vegetation coverage. The pixel and eight neighboring pixels that satisfied hypothesis 2 were selected to form equations according to (2). SVCT could be obtained by the approximate solution of equations with the least-square method.

B. Relationship Between ESA CCI Soil Moisture and SVCT

TVDI could be used to estimate surface soil moisture for the influence of thermal inertia and evaporation control on net radiation distribution [27]. TVDI is expressed as follows:

$$\text{TVDI} = (T - T_{\min}) / (T_{\max} - T_{\min}). \tag{4}$$

For the soil and vegetation components in the pixel, TVDI can be expressed as follows:

$$\text{TVDI}_{\text{soil}} = (T_s - T_{s\_\min}) / (T_{s\_\max} - T_{s\_\min}) \tag{5}$$

$$\text{TVDI}_{\text{veg}} = (T_v - T_{v\_\min}) / (T_{v\_\max} - T_{v\_\min}) \tag{6}$$

where T_s, $T_{s\_\max}$, and $T_{s\_\min}$ and T_v, $T_{v\_\max}$, and $T_{v\_\min}$ are the soil component temperature, the vegetation component temperature, and the max value and min values of soil and vegetation temperatures, respectively.

Soil moisture can be considered as the composition of soil moisture of bare soil and soil moisture under the vegetation. They can be expressed as (7) and (8), according to the negative linear relationship between TVDI and soil moisture [27]

$$\text{sm}_{\text{soil}} = a \cdot \text{TVDI}_{\text{soil}} + b \tag{7}$$

$$\text{sm}_{\text{veg}} = c \cdot \text{TVDI}_{\text{veg}} + d \tag{8}$$

where a, b, c, and d are the coefficients.

From (5)–(8), we can get the following equations:

$$\text{sm}_{\text{soil}} = a' \cdot T_s - a' \cdot T_{s\_\min} + b \tag{9}$$

$$\text{sm}_{\text{veg}} = c' \cdot T_v - c' \cdot T_{v\_\min} + d \tag{10}$$

where $a' = a/(T_{s\_\max} - T_{s\_\min})$ and $c' = c/(T_{v\_\max} - T_{v\_\min})$. $T_{s\_\max}, T_{s\_\min}, T_{v\_\max}$, and $T_{v\_\min}$ can be constant at the same time in the study area. Therefore, a' and c' can also be considered constant at the same time in the study area.

The soil moisture of pixel can be expressed as a linear combination of the soil moisture of vegetation and soil components with vegetation coverage as weight. It can be expressed as follows:

$$\text{sm} = (1 - f_c) \cdot \text{sm}_{\text{soil}} + f_c \cdot \text{sm}_{\text{veg}}. \tag{11}$$

[3][Online]. Available: http://dam.itpcas.ac.cn/chs/rs/

From (9)–(11), we can get the following:

$$\begin{aligned} \mathrm{sm} &= (1-f_c)\cdot(a'\cdot T_s - a'\cdot T_{s\_\min} + b) \\ &\quad + f_c\cdot(c'\cdot T_v - c'\cdot T_{v\_\min} + d). \end{aligned} \tag{12}$$

Eq. (12) can be expressed as follows:

$$\begin{aligned} \mathrm{sm} &= (1-f_c)\cdot a'\cdot T_s + f_c\cdot c'\cdot T_v \\ &\quad + (a'\cdot T_{s\_\min} - c'\cdot T_{v\_\min} - b + d)\cdot f_c \\ &\quad + b - a'\cdot T_{s\_\min} \end{aligned} \tag{13}$$

To simplify (13), we suppose that $m = a'\cdot T_{s\_\min} - c'\cdot T_{v\_\min} - b + d$ and $n = b - a'\cdot T_{s\_\min}$. Then, (13) can be expressed as follows:

$$\mathrm{sm} = a'\cdot(1-f_c)\cdot T_s + \cdot c' f_c\cdot T_v + m\cdot f_c + n. \tag{14}$$

T_s, T_v , and f_c can be obtained using MODIS LST and NDVI, and soil moisture can be estimated if the coefficients (a', c', m, and n) in (14) are known.

The method of upscaling soil moisture is used to obtain the coefficients in (14). The value of soil moisture with low resolution can be calculated with the average value of high-resolution soil moisture in the same area. It can be expressed as follows:

$$\mathrm{sm}_L = \frac{1}{n}\sum_{i=1}^{n}\mathrm{sm}_{\mathrm{Hi}} \tag{15}$$

where $\mathrm{sm}_{\mathrm{Hi}}$ is the soil moisture of a pixel at high resolution, and n is the number of pixels covered by the pixel at a low resolution.

From (14) and (15), we can get the following:

$$\begin{aligned} \mathrm{sm}_L &= a'\cdot\frac{1}{n}\sum_{i=1}^{n}((1-f_{ci})\cdot T_{si}) \\ &\quad + c'\cdot\frac{1}{n}\sum_{i=1}^{n} f_{ci}\cdot T_{vi} + m\cdot\frac{1}{n}\sum_{i=1}^{n} f_{ci} + n. \end{aligned} \tag{16}$$

In (16), with low resolution in ESA CCI soil moisture, the high-resolution vegetation and soil component temperatures can be estimated with MODIS MYD11A1 data in Section III-A. Furthermore, the fraction cover data, estimated with the MODIS MYD13A2 data, and the model coefficients $a', c', m, \text{and } n$ can be obtained through regression analysis with the pixels in the study area. Then, downscaled soil moisture value can be obtained with the model coefficients and high-resolution data in (14).

C. Remove the Bias

When the high-resolution soil moisture in Section III-B is upscaled with (15), the upscaled soil moisture is considered to be equal to low-resolution soil moisture. However, they are not the same for the bias in the high spatial resolution soil moisture. The bias $\mathrm{sm}_{\mathrm{bias}}$ can be expressed as follows:

$$\mathrm{sm}_{\mathrm{bias}} = \mathrm{sm}_L - \frac{1}{n}\sum_{i=1}^{n}\mathrm{sm}_{\mathrm{Hi}}. \tag{17}$$

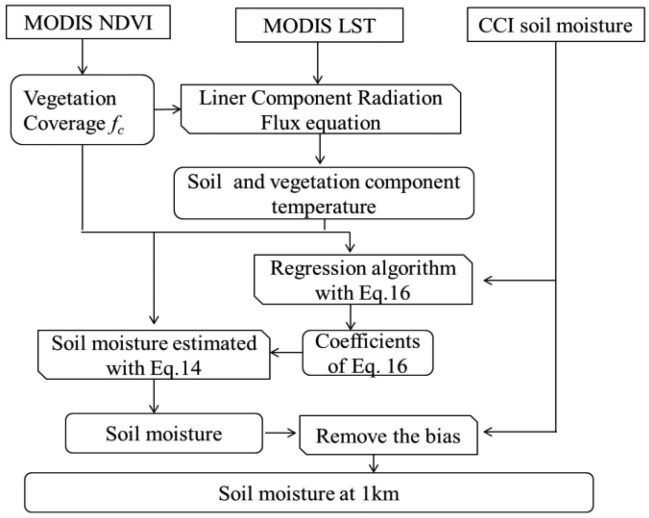

Fig. 2. Flowchart of downscaling ESA CCI soil moisture.

In order to remove the bias, the difference between ESA CCI soil moisture and the soil moisture upscaled from high-resolution data in Section III-B is derived and then resampled to high resolution with the Kriging method [44]. The final corrected downscaled soil moisture is obtained by adding the bias to the high-resolution soil moisture in Section III-B.

D. Flowchart

There are four steps implemented to downscale ESA CCI soil moisture with the MODIS LST and NDVI data. The specific downscaling steps are as follows (see Fig. 2).

First, the MODIS MYD11A1 LST data and fractional vegetation coverage obtained using the MODIS MYD13A2 NDVI data are used to estimate the vegetation and soil component temperatures via the method presented in Section III-A.

Second, the coefficients in (16) are obtained using SVCT, fractional vegetation coverage, and ESA CCI soil moisture through regression analysis.

Third, the coefficients and soil and vegetation temperatures are used to estimate high-resolution soil moisture with (14).

Finally, the bias in high-resolution soil moisture is removed using ESA CCI soil moisture with the method presented in Section III-C.

IV. Results and Discussion

A. Relationship Between ESA CCI Soil Moisture and Component Temperature

Many coarse-resolution pixels were not fully covered by high-resolution pixels due to the influence of clouds on MODIS data. In the study area, the surface was mainly covered with grassland, and the main soil type was loess. When high-resolution data were upscaled to coarse resolution with the average upscaling algorithm, the upscaled coarse-resolution pixels that were covered by high-resolution pixels with a percentage higher than 70% were considered to be fully covered by high-resolution pixels.

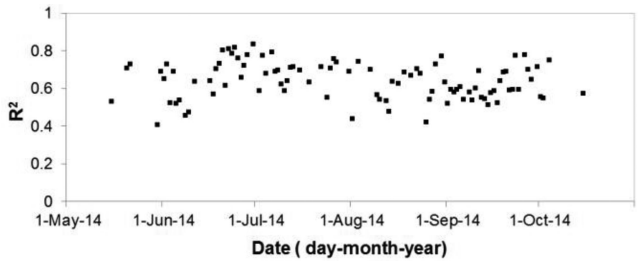

Fig. 3. Time series of coefficients of determination using (16) from May to October 2014.

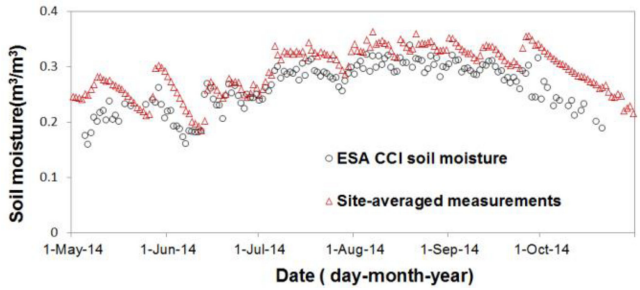

Fig. 4. Time series of ESA CCI soil moisture and site-averaged measurements from the SMTMN on the Tibetan Plateau from May to October 2014.

When coverage of the coarse-resolution pixels across the study area was higher than 60%, the data of these days were applied with the method.

SVCT were estimated with the method presented in Section II-A. The vegetation coverage calculated from the MODIS data was used to form (16), and the coefficients of (14) and (16) were obtained through regression analysis. Fig. 3 shows the time series diagram of the regression model (16) coefficients of determination.

As liquid soil water was frozen during the frozen season from November to March of the following year, data were selected during the unfrozen period. According to the thresholds, cloudy pixels in MODIS LST and invalid pixels in ESA CCI soil moisture were excluded from May to October 2014 (see Fig. 3). The determination coefficient R^2 of (16) was higher than 0.5 on most days of the study period, especially from late June to early July when R^2 is higher than 0.6. One reason is that ESA CCI soil moisture was more consistent with ground measurements from late June to early July than on other days of the study period (see Fig. 4). In general, the relationship between ESA CCI soil moisture and component temperature using (16) is stable to downscale ESA CCI soil moisture, especially when ESA CCI soil moisture was more consistent with ground measurements during the study period.

The statistic of coefficients is shown in Table I. The negative correlation between soil moisture and SVCT and the positive correlation between soil moisture and fractional coverage could be confirmed by the coefficients. The values of a' and c' were negative on most days. The days when the values of a' and c' were positive were almost in early May, late September, and October.

TABLE I
COEFFICIENTS STATISTIC OF (14) FROM MAY TO OCTOBER 2014

	a'	c'	m	n
average	-0.053	-0.018	0.310	0.052
variance	0.128	0.011	0.111	0.044
maximum	0.758	0.216	1.510	0.743
minimum	-0.941	-0.275	0.008	-0.634

One of the reasons was that this period was just at the beginning (late September and October) or in the end (early May) of the freeze–thaw period. Soil moisture thawed with the increase in temperature in early May, and soil moisture froze with the decrease in temperature in late September and October. Thus, the soil might become wet with the increase in temperature. However, the variance of the coefficients is large, especially the variance of a'. This might be caused by the uncertainty of the derived SVCT.

B. Downscaled Soil Moisture

With the coefficients and high-resolution soil and vegetation temperature data in (14), downscaled soil moisture could be estimated, and the bias was removed with the method presented in Section III-C.

Fig. 5 shows an example of the spatial distribution of ESA CCI soil moisture and downscaled soil moisture on June 4, July 27, and September 19, 2014. The distribution of ESA CCI soil moisture and downscaled soil moisture was consistent with wet east and dry west distribution characteristics, especially on June 4. Vegetation is in the growing season in May and June and in wilts in October, and soil moisture was lower on June 4 than on July 27 and September 19. The distribution of the soil moisture was similar on September 19 and July 27, except for the western regions. Soil moisture was higher in the western region on September 19 than on July 27.

C. Compare With In Situ *Soil Moisture at the Site Scale*

Downscaled soil moisture is compared with the ground observation data to further analyze the effectiveness of the downscaling method.

Before comparing the downscaled soil moisture with the ground measurements, SVCT were compared with the temperature observed at the 5 cm depth, as shown in Fig. 6 and Table I. It can be seen that the soil and vegetation temperatures were higher from June to September and lower in May and October at the five sites in Fig. 6. Furthermore, R^2 was higher than 0.45, except for the soil temperature at site M19 with 0.38 for soil component temperature, as shown in Table I. Compared with the soil component temperature and MYD11A1 LST in Table II, R^2 of the vegetation component temperature was higher. Most of the soil component temperatures and vegetation component temperatures were higher than the ground measurements of the soil temperature at 5 cm depth, and the soil component temperature was higher than the vegetation component temperature.

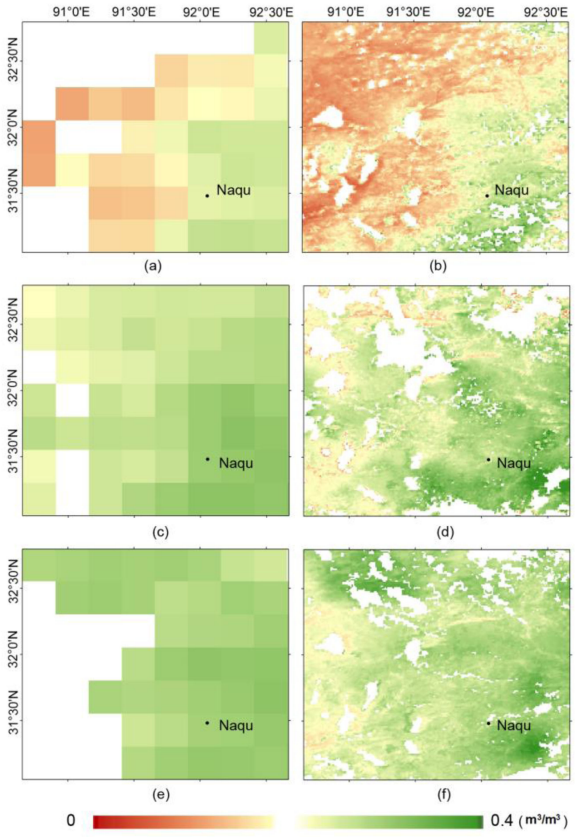

Fig. 5. ESA CCI soil moisture at 25-km spatial resolution and downscaled soil moisture at 1-km spatial resolution in Naqu area on the Tibetan Plateau on (a) and (b) June 4; (c) and (d) July 27; and (e) and (f) September 19, 2014.

TABLE II
R^2 OF SVCT AND MYD11A1 LST WITH GROUND MEASUREMENTS OF TEMPERATURE AT THE FIVE SITES

Site	Soil component temperature	Vegetation component temperature	MODIS LST
M10	0.47	0.65	0.52
M11	0.48	0.62	0.52
M14	0.57	0.65	0.58
M19	0.38	0.59	0.40
M21	0.46	0.64	0.48

One of the reasons is that the MODIS LST, which is used to estimate SVCT, can only monitor the LST. The temperature at a depth of 5 cm, where the *in situ* temperature was observed, was lower than the LST during the day when the MODIS MYD11A1 LST was observed at about 1:00 to 2:00 PM. Therefore, SVCT obtained using the MODIS MYD11A1 LST were higher than the *in situ* measurements at a depth of 5 cm. Meanwhile, according to the method of estimating SVCT and hypothesis 2 suggesting that vegetation component temperature is lower than the soil component temperature in Section III, the MODIS LST, which is higher from June to September and lower in May and October, caused the same for SVCT.

The time series of downscaled soil moisture was compared with *in situ* measurements between May and October 2014 (see Fig. 6). Based on ground measurements, the soil moisture conditions ranged from dry (0.15 m^3/m^3) in May and October to wet (0.4 m^3/m^3) from June to September at most of the five sites, except for site M19 with a range of soil moisture from 0.08 to 0.27 m^3/m^3. The trends of the downscaled soil moisture were similar to the trends of ground measurements, with high levels from June to September and lower levels in May and October at the five sites. However, the soil moisture was generally underestimated at most of the sites [see Fig. 6(a)–(e)], except at M19 [see Fig. 6(d)]. Errors of downscaled soil moisture in the premonsoon (from May to mid-June) and decay seasons (after September) were higher than in the growing season (mid-June to September).

The underestimation of ESA CCI soil moisture during this period (see Fig. 4) is an important reason for the underestimation of downscaled soil moisture. One reason for the errors of the downscaled soil moisture during the premonsoon season (from May to mid-June) and the decay season (October) is that ESA CCI soil moisture was less consistent with ground measurements during this period than that from mid-June to September (see Fig. 4). R^2 of between ESA CCI soil moisture and ground measurements was 0.4 with root-mean-square error (RMSE) being 0.064 m^3/m^3 during this period under the condition of NDVI lower than 0.4 in Fig. 7. However, the study area was almost bare soil and covered by sparse vegetation, with NDVI lower than 0.4 at the five sites during this period. Meanwhile, the experiential data of soil emissivity were used to simplify the method of estimating the component temperature. The experiential data used in this study may not be suitable for the conditions when the surface gradually becomes wet from the frequent rainfall from May to mid-June and the freeze–thaw period in October. This may cause the error in the soil component temperature and downscaled soil moisture to be large during this period. As for site M19, the values of NDVI and ground measurements of temperature were similar to the other four sites. However, soil moisture was drier at site M19 than at the other sites (see Fig. 6). A possible reason could be that the ground measurements at site M19 could not represent the value of the pixel at 1 km located by site M19, and the difference between the downscaled soil moisture and ground measurements is large at site M19 in Fig. 6(d).

As TVDI was suitable for monitoring soil moisture in middle and high vegetation fraction regions [41], [42], the downscaled soil moisture under the condition of the NDVI values higher than 0.4 was further analyzed and compared with ground measurements in Table III. R^2 was higher than 0.4 and RMSE was less than 0.07 m^3/m^3 at most of the sites, except at M19 (Table III). The value of RMSE was 0.76 m^3/m^3 at site M19, with the lowest value of R^2 being 0.23. Besides the possible reason that site M19 may not have represented the pixel that the site located, the errors of SVCT (in Table I) contributed to the errors of the downscaled soil moisture. Considering the accuracy of ESA CCI soil moisture shown in Fig. 7, the method was sufficient, with RMSE being 0.0568 m^3/m^3 under the conditions of NDVI higher than 0.4.

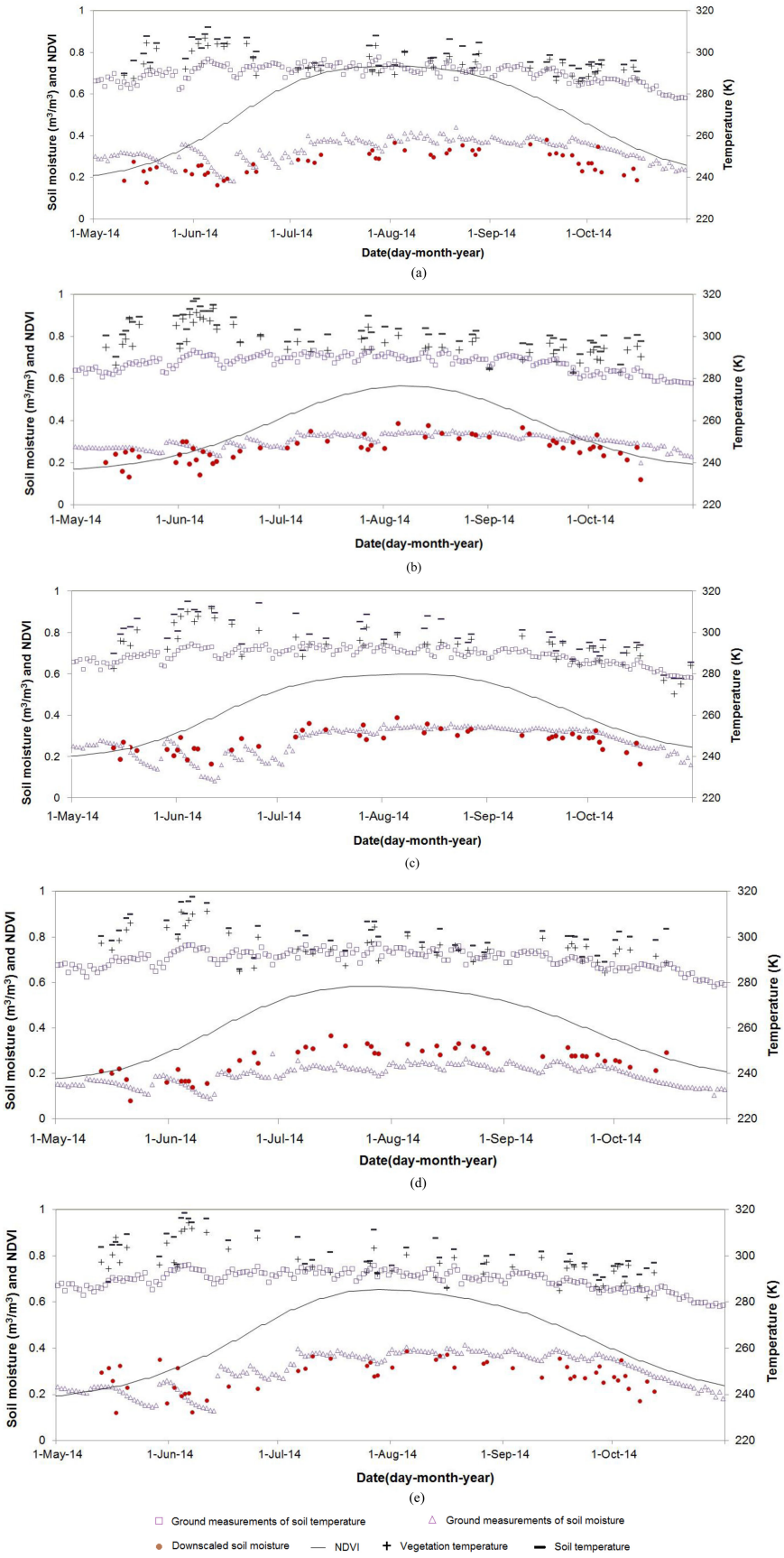

Fig. 6. Time series of downscaled soil moisture and ground measurement, NDVI in the left axis and vegetation and soil temperatures in the right axis at (a) site M10, (b) site M11, (c) site M14 (d) M19, and (e) site M21 during the period of May to October 2014.

TABLE III
R^2 AND RMSE BETWEEN DOWNSCALED SOIL MOISTURE AND GROUND MEASUREMENTS OF SOIL MOISTURE FOR THE PERIOD FROM MAY TO OCTOBER 2014 UNDER THE CONDITION OF NDVI HIGHER THAN 0.4

Site	SVCT		TVDI		Triangle-based empirical	
	R^2	RMSE (m^3/m^3)	R^2	RMSE (m^3/m^3)	R^2	RMSE (m^3/m^3)
M10	0.51	0.068	0.49	0.065	0.41	0.084
M11	0.38	0.041	0.46	0.055	0.22	0.061
M14	0.53	0.047	0.65	0.051	0.42	0.066
M19	0.23	0.076	0.36	0.067	0.29	0.096
M21	0.42	0.061	0.44	0.054	0.31	0.087
5 sites	0.44	0.0568	0.454	0.0602	0.33	0.0788

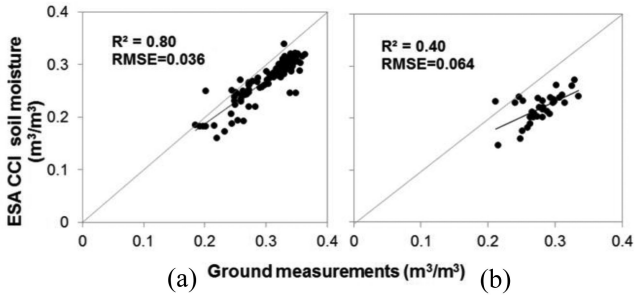

Fig. 7. Comparison of ESA CCI soil moisture and ground measurements from the SMTMN on the Tibetan Plateau under the conditions of (a) NDVI higher than 0.4 and (b) NDVI lower than 0.4.

The results of the proposed method were compared with the downscaled soil moisture based on TVDI and the triangle-based empirical method in Table III. The triangle-based empirical method was proposed by Choi and Hur [45] and has been testified in the Tibetan Plateau [42].

The results showed that the performances of the three methods were better at sites M10 and M14 and worse at sites M19 and M11 than other sites. But the value of R^2 with the triangle-based empirical method was lower than the other two methods, with RMSE higher than 0.07 m^3/m^3. For the five sites as a whole, the correlation between *in situ* measurements and the results of the TVDI-based method and the SVCT-based method was similar with R^2 higher than 0.4, and the RMSE of the SVCT-based method was lower with 0.0568 m^3/m^3 than the TVDI-based method with 0.0602 m^3/m^3.

In general, the trends of the downscaled soil moisture are similar to ground measurements under conditions when NDVI values are higher than 0.4. Compared with the method based on TVDI, the method could be used to downscale soil moisture without knowing the dry and wet lines, which were used to estimate TVDI.

Errors in the ESA CCI soil moisture at 25 km and the component temperature at 1 km are the reasons that cause the uncertainties in the downscaled soil moisture. In order to estimate SVCT with a simple method, the hypothesis that the SVCT of adjacent pixels were close was made. Pixels with a negative correlation between LST and vegetation coverage were selected to estimate SVCT. This would reduce the uncertainty of the results to a certain extent. The uncertainty of NDVI, the method to estimate fraction coverage, and the hypothesis that the SVCT are close would result in an error in estimating SVCT.

V. CONCLUSION

This study presented a method of downscaling the ESA CCI 25-km soil moisture product using soil and vegetation temperatures derived from MODIS LST and NDVI data. The method of estimating SVCT assumes that the vegetation and soil component temperatures of adjacent pixels are close and the soil component temperature is lower than the vegetation component temperature for the same pixel. The relationship between soil moisture and component temperature was built based on monitoring the soil moisture with TVDI. Furthermore, the coefficients could be obtained directly from ESA CCI soil moisture at 25 km and soil and the vegetation component temperatures at 1 km with the method based on the upscaling algorithm of the soil moisture. The method was applied to the Naqu area on the Tibetan Plateau of China. The results were compared with the ground measurements at five sites of TP-SMTMN in Naqu with the average RMSE being 0.058 m^3/m^3. Similar results have been shown with the method based on TVDI. That means the proposed method could downscale CCI soil moisture without estimating the dry and wet lines, which were used to estimate TVDI.

Considering the factors that influence the downscaled results, the accuracy of ESA CCI soil moisture, and SVCT are important. To simplify the method, we assume that the vegetation and soil component temperatures of eight adjacent pixels are close and the emissivities of the soil and vegetation are taken to be constant. This may not be true for areas with different soil textures and covered with different kinds of vegetation. In order to reduce the uncertainty of the SVCT, only the pixels with a negative correlation between the surface temperature and vegetation coverage were selected to estimate the SVCT. Although the coarse-resolution pixels that were covered by high-resolution pixels with a percentage higher than 70% were considered to be fully covered by high-resolution pixels to reduce the influence of clouds, it might not be the true when the surface coverage is complex and heterogeneous. Research studies on NDVI and LST reconstruction can fill the data gaps caused by cloud cover [42], [46], [47], which would improve the application of the proposed method. When removing the bias of the downscaled soil moisture, the Kriging method was applied in this study. Other methods, such as the self-adaptive window method [48],

could be used and analyzed in further study to improve the results. Meanwhile, the uncertainty of input data, such as NDVI, LST, and the elevation variations, also influences the results.

The method is more applicable to areas with an NDVI higher than 0.4. Further studies can focus on the method of estimating SVCT, such as the method using a single thermal channel [49]. The methods of downscaling soil moisture under different conditions should also be studied, such as merging different approaches for downscaling soil moisture, such as the method based on ATI [44] that could be used under the condition of a bare surface or in a sparsely vegetated area.

REFERENCES

[1] C. Champagne, A. Berg, J. White, S. Belair, and M. Carrera, "Impact of soil moisture data characteristics on the sensitivity to crop yields under drought and excess moisture conditions," *Remote Sens.*, vol. 11, no. 4, Feb. 2019, Art. no. 372.

[2] D. G. Miralles, T. R. H. Holmes, R. A. M. De Jeu, J. H. Gash, A. G. C. A. Meesters, and A. J. Dolman, "Global land-surface evaporation estimated from satellite-based observations," *Hydrol. Earth. Syst. Sci.*, vol. 15, no. 5, pp. 453–469, Oct. 2010.

[3] S. I. Seneviratne *et al.*, "Investigating soil moisture–climate interactions in a changing climate: A review," *Earth-Sci. Rev.*, vol. 99, no. 3/4, pp. 125–161, May 2010.

[4] M. Pablos, J. Martínez-Fernandez, M. Piles, N. Sánchez, M. Vall-llossera, and A. Camps, "Multi-temporal evaluation of soil moisture and land surface temperature dynamics using in situ and satellite observations," *Remote Sens.*, vol. 8, no. 7, 2016, Art. no. 587.

[5] K. Das and P. K. Paul, "Present status of soil moisture estimation by microwave remote sensing," *Cogent Geosci.*, vol. 1, no. 1, 2015, Art. no. 1084669.

[6] H. E. Beck *et al.*, "Evaluation of 18 satellite- and model-based soil moisture products using in situ measurements from 826 sensors," *Hydrol. Earth Syst. Sci.*, vol. 25, no. 1, pp. 17–40, Jan. 2021.

[7] R. A. M. de Jeu, W. Wagner, T. R. H. Holmes, A. J. Dolman, N. C. van de Giesen, and J. Friesen, "Global soil moisture patterns observed by space borne microwave radiometers and scatterometers," *Surv. Geophys.*, vol. 29, no. 4, pp. 399–420, Oct. 2008.

[8] B. P. Mohanty, M. H. Cosh, V. Lakshmi, and C. Montzka, "Soil moisture remote sensing: State-of-the-science," *Vadose Zone J.,* vol. 16, no. 1. Jan. 2017.

[9] E. G. Njoku, T. J. Jackson, V. Lakshmi, T. K. Chan, and S. V. Nghiem, "Soil moisture retrieval from AMSR-E," *IEEE Trans. Geosci. Electron.*, vol. 41, no. 2, pp. 215–229, Mar. 2003.

[10] H. Fujii, T. Koike, and K. Imaoka, "Improvement of the AMSR-E algorithm for soil moisture estimation by introducing a fractional vegetation coverage dataset derived from MODIS data," *J. Remote Sens. Soc. Jpn.*, vol. 29, no. 1, pp. 282–292, 2009.

[11] Y. H. Kerr, F. Secherre, J. Lastenet, and J. P. Wigneron, "SMOS: Analysis of perturbing effects over land surfaces," *Proc. IEEE Int. Geosci. Remote Sens. Symp.*, Toulouse, France, 2003, pp. 908–910.

[12] C. S. Kang *et al.*, "Global soil moisture retrievals from the Chinese FY-3D microwave radiation imager," *IEEE Trans. Geosci. Remote Sens.*, vol. 59, no. 5, pp. 4018–4032, May 2021.

[13] D. Entekhabi *et al.*, "The soil moisture active passive (SMAP) mission," *IEEE Proc.*, vol. 98, no. 5, pp. 704–716, May 2010.

[14] W. Dorigo *et al.*, "ESA CCI soil moisture for improved earth system understanding: State-of-the art and future directions," *Remote Sens.,* vol. 203, pp. 185–215, Dec. 2017.

[15] A. Gruber, T. Scanlon, R. Van Der Schalie, W. Wagner, and W. Dorigo, "Evolution of the ESA CCI soil moisture climate data records and their underlying merging methodology," *Earth Syst. Sci. Data*, vol. 11, no. 2, pp. 717–739, May 2019.

[16] N. Nicolai-Shaw, J. Zscheischler, M. Hirschi, L. Gudmundsson, and S. I. Seneviratne, "A drought event composite analysis using satellite remote-sensing based soil moisture," *Remote Sens. Environ.*, vol. 203, pp. 216–225, Dec. 2017.

[17] L. Ciabatta *et al.*, "SM2RAIN-CCI: A new global long-term rainfall data set derived from ESA CCI soil moisture," *Earth Syst. Sci. Data*, vol. 10, no. 1, pp. 1–23, Sep. 2017.

[18] W. T. Crow and E. F. Wood, "The value of coarse-scale soil moisture observations for regional surface energy balance modeling," *J. Hydrometeorol.*, vol. 3, no. 4, pp. 467–482, 2002.

[19] N. Chauhan, S. Miller, and P. Ardanuy, "Spaceborne soil moisture estimation at high resolution: A microwave-optical/IR synergistic approach," *Int. J. Remote Sens.*, vol. 24, no. 22, pp. 4599–4622, Sep. 2002.

[20] Y. Yang *et al.*, "Estimation of surface soil moisture from thermal infrared remote sensing using an improved trapezoid method," *Remote Sens.*, vol. 7, no. 7, pp. 8250–8270, 2015.

[21] E. Babaeian, M. Sadeghi, T. E. Franz, S. Jones, and M. Tuller, "Mapping soil moisture with the OPtical TRApezoid model (OPTRAM) based on long-term MODIS observations," *Remote Sens. Environ.*, vol. 211, pp. 425–440, 2018.

[22] O. Merlin, A. Chehbouni, G. Boulet, and Y. Kerr, "Assimilation of disaggregated microwave soil moisture into a hydrologic model using coarse-scale meteorological data," *J. Hydrometeorol.*, vol. 7, no. 6, pp. 1308–1322, Dec. 2006.

[23] O. Merlin, Y. Malbéteau, Y. Notfi, S. Bacon, S. Khabba, and L. Jarlan, "Performance metrics for soil moisture downscaling methods: Application to DISPATCH data in central Morocco," *Remote Sens.,* vol. 7, no. 4, pp. 3783–3807, Mar. 2015.

[24] S. B. Duan and Z. L. Li, "Spatial downscaling of MODIS land surface temperatures using geographically weighted regression: Case study in northern China," *IEEE Trans. Geosci. Remote Sens.*, vol. 54, no. 11, pp. 6458–6469, Nov. 2016.

[25] Y. Liu, Y. Yang, W. Jing, and X. Yue, "Comparison of different machine learning approaches for monthly satellite-based soil moisture downscaling over Northeast China," *Remote Sens.*, vol. 10, no. 1, 2018, Art. no. 31.

[26] J. Peng, A. Loew, S. Zhang, J. Wang, and J. Niesel, "Spatial downscaling of satellite soil moisture data using a vegetation temperature condition index," *IEEE Trans. Geosci. Remote Sens.*, vol. 54, no. 1, pp. 558–566, Jan. 2016.

[27] I. Sandholt, K. Rasmussen, and J. Andersen, "A simple interpretation of the surface temperature/vegetation index space for assessment of surface moisture status," *Remote. Sens. Environ.*, vol. 79, no. 2/3, pp. 213–224, Feb. 2002.

[28] J. Kovačević, Ž. Cvijetinović, N. Stančić, N. Brodić, and D. Mihajlović, "New downscaling approach using ESA CCI SM products for obtaining high resolution surface soil moisture," *Remote Sens.*, vol. 12, no. 1119, pp. 1–32, 2020.

[29] W. Zhao, F. Wen, Q. Wang, N. Sanchez, and M. Piles, "Seamless downscaling of the ESA CCI soil moisture data at the daily scale with MODIS land products," *J. Hydrol.*, vol. 603, 2021, Art. no. 126930.

[30] E. G. Njoku *et al.*, "Observations of soil moisture using a passive and active low-frequency microwave airborne sensor during SGP99," *IEEE Trans. Geosci. Remote Sens.*, vol. 40, no. 12, pp. 2659–2673, Dec. 2002.

[31] U. Narayan and V. Lakshmi, "Characterizing subpixel variability of low resolution radiometer derived soil moisture using high resolution radar data," *Water Resour. Res.*, vol. 44, no. 6, pp. 2389–2393, Jun. 2008.

[32] U. Narayan, V. Lakshmi, and T. J. Jackson, "High-resolution change estimation of soil moisture using L-band radiometer and radar observations made during the SMEX02 experiments," *IEEE Trans. Geosci. Remote Sens.*, vol. 44, no. 6, pp. 1545–1554, Jun. 2006.

[33] M. Piles, D. Entekhabi, and A. Camps, "A change detection algorithm for retrieving high-resolution soil moisture from SMAP radar and radiometer observations," *IEEE Trans. Geosci. Remote Sens.*, vol. 47, no. 12, pp. 4125–4131, Dec. 2009.

[34] B. Fang, V. Lakshmi, T. J. Jackson, R. Bindlish, and A. Colliander, "Passive/active microwave soil moisture change disaggregation using SMAPVEX12 data," *J. Hydrol.*, vol. 574, pp. 1085–1098, 2019.

[35] N. N. Das, D. Entekhabi, and E. G. Njoku, "An algorithm for merging SMAP radiometer and radar data for high-resolution soil-moisture retrieval," *IEEE Trans. Geosci. Remote Sens.*, vol. 49, no. 5, pp. 1504–1512, May 2011.

[36] N. N. Das, D. Entekhabi, E. G. Njoku, J. J. Shi, J. T. Johnson, and A. Colliander, "Tests of the SMAP combined radar and radiometer algorithm using airborne field campaign observations and simulated data," *IEEE Trans. Geosci. Remote Sens.*, vol. 52, no. 4, pp. 2018–2028, Apr. 2014.

[37] M. Piles, G. P. Petropoulos, N. Sanchez, A. Gonzalez-Zamora, and G. Ireland, "Towards improved spatio-temporal resolution soil moisture retrievals from the synergy of SMOS and MSG SEVIRI spaceborne observations," *Remote Sens. Environ.*, vol. 180, pp. 403–417, Jul. 2016.

[38] M. L. Coleman and J. D. Niemann, "Controls on topographic dependence and temporal instability in catchment-scale soil moisture patterns," *Water Resour. Res.*, vol. 49, no. 3, pp. 1625–1642, Mar. 2013.
[39] K. J. Ranney, J. D. Niemann, B. M. Lehman, T. R. Green, and A. S. Jones, "A method to downscale soil moisture to fine resolutions using topographic, vegetation, and soil data," *Adv. Water Resour.*, vol. 76, pp. 81–96, Feb. 2015.
[40] F. A. Busch, J. D. Niemann, and M. Coleman, "Evaluation of an empirical orthogonal function-based method to downscale soil moisture patterns based on topographical attributes," *Hydrol. Processes*, vol. 26, no. 18, pp. 2696–2709, Aug. 2012.
[41] G. Petropoulos , T. N. Carlson, M. J. Wooster, and S. Islam, "A review of Ts/VI remote sensing based methods for the retrieval of land surface energy fluxes and soil surface moisture," *Prog. Phys. Geogr.*, vol. 33, pp. 224–250, 2009, doi: 10.1177/0309133309338997.
[42] W. Zhao and A. Li, "A comparison study on empirical microwave soil moisture downscaling methods based on the integration of microwave-optical/IR data on the Tibetan Plateau," *Int. J. Remote Sens.*, vol. 36, no. 19, pp. 4986–5002, Jun. 2015.
[43] K. Yang *et al.*, "A multi-scale soil moisture and freeze–thaw monitoring network on the third pole," *Bull. Amer. Meteorol. Soc.*, vol. 94, pp. 1907–1916, Dec. 2013.
[44] C. Song and L. Jia, "A method for downscaling Fengyun-3B soil moisture based on apparent thermal inertia," *Remote Sens.*, vol. 6, pp. 1–15, 2014.
[45] M. Choi and Y. Hur, "A microwave-optical/infrared disaggregation for improving spatial representation of soil moisture using AMSR-E and MODIS products," *Remote Sens. Environ.*, vol. 124, pp. 259–269, Sep. 2012.
[46] A. F. Militino, M. D. Ugarte, U. Pérez-Goya, and M. G. Genton, "Interpolation of the mean anomalies for cloud filling in land surface temperature and normalized difference vegetation index," *IEEE Trans. Geosci. Remote Sens.*, vol. 57, no. 8, pp. 6068–6078, Aug. 2019.
[47] G. Yang, W. Sun, H. Shen, X. Meng, and J. Li, "An integrated method for reconstructing daily MODIS land surface temperature data," *IEEE J. Sel. Topics Appl. Earth Observ. Remote Sens.*, vol. 12, no. 3, pp. 1026–1040, Mar. 2019, doi: 10.1109/JSTARS.2019.2896455.
[48] F. Wen, W. Zhao, Q. Wang, and N. Sánchez, "A value-consistent method for downscaling SMAP passive soil moisture with MODIS products using self-adaptive window," *IEEE Trans. Geosci. Remote Sens.*, vol. 58, no. 2, pp. 913–924, Feb. 2020, doi: 10.1109/TGRS.2019.2941696.
[49] W. Zhan, Y. Chen, J. Zhou, and J. Li, "An algorithm for separating soil and vegetation temperatures with sensors featuring a single thermal channel," *IEEE Trans. Geosci. Remote Sens.*, vol. 49, no. 5, pp. 1796–1809, May 2011, doi: 10.1109/TGRS.2010.2082555.

Chengyun Song received the Ph.D. degree in cartography and geography information system from the Institute of Remote Sensing and Digital Earth, Chinese Academy of Sciences, Beijing, China, in 2014.

He is a Lecturer with the Anhui University of Science & Technology, Huainan, China. His research interests include microwave remote sensing of soil moisture and soil moisture downscaling algorithm.

Guangcheng Hu received the Ph.D. degree in groundwater science and engineering from the China University of Geosciences, Beijing, China, in 2010.

He is an Assistant Researcher with the Aerospace Information Research Institute, Chinese Academy of Sciences, Beijing, China. He was a Postdoctoral Fellow with the Institute of Remote Sensing and Digital Earth, Chinese Academy of Sciences, from 2010 to 2014. His research interests include remote-sensing-based evapotranspiration and soil moisture estimation.

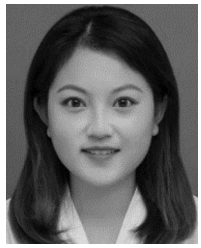

Yanli Wang received the bachelor's degree in geographic information science from Taiyuan Normal University, Jinzhong, China, in 2019. She is currently working toward the master's degree in surveying and mapping engineering with the Anhui University of Science and Technology, Huainan, China.

Her main research interest includes thermal infrared remote sensing. She is committed to the innovation and application of different multichannel land surface temperature inversion methods.

Xueshan Qu received the bachelor's degree in surveying and mapping engineering from the Hebei University of Engineering, Handan, China, in 2019. She is currently working toward the master's degree in surveying and mapping science and technology with the Anhui University of Science and Technology, Huainan, China.

Her main research interest includes exploring the method of fine classification of crops by using multi-source remote sensing data.